ELSEVIER

Contents lists available at ScienceDirect

Materials Today Physics

journal homepage: www.journals.elsevier.com/materials-today-physics





Experimental observation of geometric effect on the electron diffraction of quasi-one-dimensional nanostructures

Tongxie Zhang ^a, Adam T. Eaton ^a, Dibya K. Mukherjee ^a, Michael Cao ^b, Amanda L. Coughlin ^a, Thomas Ruch ^a, Xun Zhan ^c, Hanyu Zhu ^b, Yimo Han ^b, Herbert A. Fertig ^{a,d,e,**}, Shixiong Zhang ^{a,e,*}

- ^a Department of Physics, Indiana University, Bloomington, IN, 47405, United States
- b Department of Materials Science and NanoEngineering, Rice University, Houston, TX, 77005, United States
- ^c Electron Microscopy Center, Indiana University, Bloomington, IN, 47405, United States
- d Instituto de Ciencia de Materiales de Madrid, (CSIC), Cantoblanco, 28049, Madrid, Spain
- ^e Quantum Science and Engineering Center, Indiana University, Bloomington, IN, 47405, United States

ARTICLE INFO

Keywords: One-dimensional nanostructures Topological materials Geometric effects Electron diffraction

ABSTRACT

One-dimensional (1D) nanostructures, such as nanowires, constitute building blocks for nanoscience and nanotechnology. Their fundamental physical properties are dictated by their crystalline structures, which are often characterized by transmission electron microscopy (TEM). Theoretically, the shape of a nanostructure can affect its electron diffraction pattern; however, for 1D nanostructures, an experimental observation of this geometric effect has not been reported. Here, we demonstrate unambiguously the first experimental observation of this geometric effect in electron diffraction from nanowires of iridium dioxide (IrO_2) and lead tin telluride ($\text{Pb}_{1-x}\text{Sn}_x\text{Te}$), which are topological semimetals and topological crystalline insulators, respectively. Grown by chemical vapor deposition, the nanowires are single-crystalline and have well defined facets with nearly rectangular cross-sections. Diffraction spot splitting was observed in electron diffraction patterns when the e-beam was not perpendicular to the major facets of the nanowires. Atomic-resolution scanning TEM studies rule out other possible origins of the splitting, including twin domains and non-uniform strain. Theoretical calculations of electron diffraction capturing the nanowire geometry show good agreement with the experimental results, including the diffraction order dependence of the peak splitting. The observation of this geometric effect offers a non-destructive approach to characterizing the thickness of the one-dimensional nanostructures.

1. Introduction

One-dimensional (1D) nanostructures, such as nanowires/nanobeams, have been a subject of intense study in nanoscience and nanotechnology for decades due to their unique physical and chemical properties, offering great potential for applications in nanoelectronics [1–4], optoelectronics [5,6], catalysis [7–10], energy harvesting and storage [11–15], and information technology [16,17]. The extraordinary properties of nanowires compared to their bulk counterparts commonly originate from the 1D confinement and their large surface-area-to-volume ratios [18], both of which are dependent on the shape and size of the nanowire cross-section. For example, the cross-sectional geometries of gold nanowires have a strong influence on

the surface plasmon polariton they support [19]. The catalytic [20,21], mechanical [22,23], and thermal transport [24–26] properties of nanowires are also shape- and size-dependent. For topological materials, the characterization of a nanowire's cross-sectional geometry and the orientations of its surfaces are very important, as some topological surface states exist only on certain crystalline surfaces [27–29].

The crystalline structure of an *individual* nanowire is typically characterized by transmission electron microscopy (TEM) [30–32], as the small volume involved is not suitable for bulk structural characterizations such as neutron scattering or X-ray diffraction. In standard electron diffraction of an ideal crystal, a set of diffraction peaks are produced by the reflections which satisfy the Laue condition in reciprocal space. In the kinematical approximation in which one assumes the electron beam

^{*} Corresponding author. Department of Physics, Indiana University, Bloomington, IN, 47405, United States.

^{**} Corresponding author. Department of Physics, Indiana University, Bloomington, IN, 47405, United States. *E-mail addresses*: hfertig@indiana.edu (H.A. Fertig), sxzhang@indiana.edu (S. Zhang).

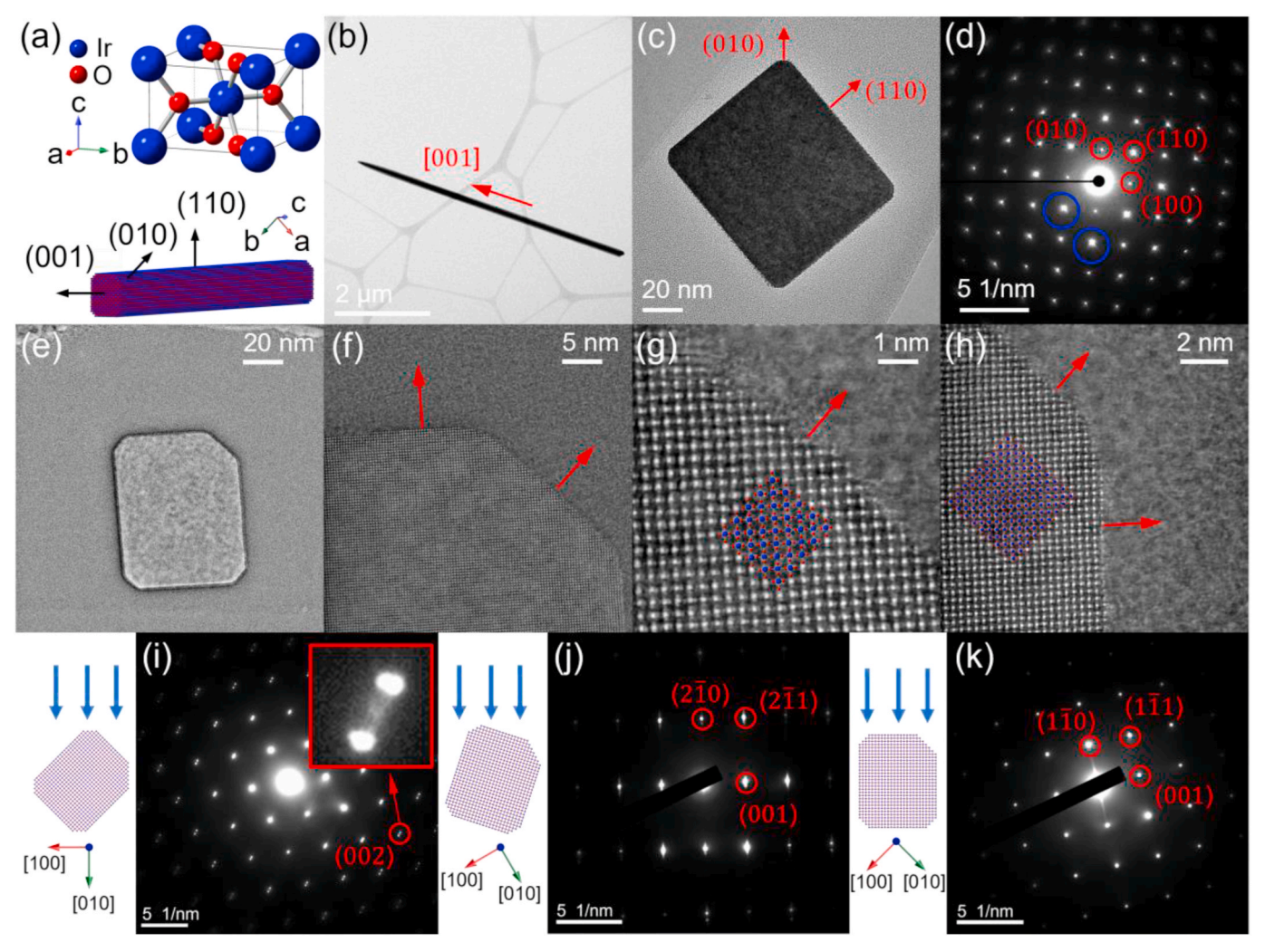


Fig. 1. (a) A tetragonal crystal structure of IrO₂ (top panel) and a schematic picture showing the shape and the surface orientation of a IrO₂ nanowire. Low magnification TEM images of IrO₂: (b) top view with the e-beam perpendicular to the nanowire axis and (c) cross-sectional view with the beam parallel to the axis of another nanowire. The nanowire in (c) was cut into a thin slice by a focused ion beam. (d) A SAED pattern taken with the e-beam along the nanowire axis (i.e., [001]). Streaks in perpendicular directions are observed in diffraction spots, and blue circles indicate two examples. (e)–(h) Optimum bright field images showing the cross-section of a nanowire at different scales. SAED patterns acquired in the (i) [010], (j) [120], and (k) [110] zone axes. The panels on the left illustrate the relative orientation of the e-beam and the crystallographic axis. The inset in (i) shows the clear splitting at (002) diffraction spot as an example.

is scattered only once, the structure of a finite crystal in reciprocal space is described by a convolution of the Fourier transforms of the crystal lattice and the crystal shape [33]. The observed diffraction pattern is a projection of the intersection of the Ewald sphere with the crystal reciprocal structure, where the radius of the Ewald sphere is $1/\lambda$, with λ the electron wavelength. Qualitatively, the Fourier transform of a finite crystal is a set of reciprocal-lattice rods (or relrods), with orientations perpendicular to each surface of the crystal. The length and width of these relrods are inversely proportional to the sharpness and size of the corresponding side surface, respectively. Within each relrod are intensity oscillations due to interference of the diffraction from different surfaces. Given the small size of nanowires in their radial directions, this geometric effect is anticipated to play a significant role in electron diffraction; nevertheless, to the best of our knowledge, there has not been an unambiguous experimental observation of this effect, even as nanowires have been studied for several decades.

Here, we have experimentally demonstrated, for the first time, a cross-sectional geometric effect on the electron diffraction of nanowires which may offer a facile, non-destructive method to characterize the cross-sectional shapes and sizes of nanowires. Our studies were focused on single-crystalline nanowires with well-defined side surfaces of two

representative topological materials: the topological semimetal IrO_2 [34–38] and the topological crystalline insulator (PbSn)Te [39–42]. We observed the effect in selected-area electron diffraction (SAED) patterns, which manifested itself by a splitting of the diffraction spots. Theoretical simulations resemble the fine structure of the observed splitting based on the geometric effect described above.

2. Experimental and calculation details

2.1. Nanowire synthesis

The synthesis of iridium oxide (IrO₂) nanowires was carried out in a three-zone quartz tube furnace -based chemical vapor deposition (CVD) system. While zone 1 of the furnace was vacant, IrO₂ powder (Alfa Aesar, 99.99% metals basis) was placed in an alumina boat in the center of zone 2. Four silicon substrates were cut from wafers at a length of $\sim \! 3$ in each and were evenly coated with a solution of sonicated IrO₂ powder in IPA. The silicon wafers were placed immediately after the IrO₂ powder boat and extended $\sim \! 0.5 \! - \! 12.5$ inches downstream from zone 2 into zone 3. The growth temperatures of zone 1, 2, and 3 were 550, 950, and 600 °C, respectively, and the pressure of the quartz tube was set to

900 Torr and was maintained throughout the growth. During the ramping segment of the growth, a 10 sccm flow of Ar gas was used as the initial carrier gas during the ramping up segment and, once the growth temperatures were reached, O2 gas was introduced (in addition to the Ar gas) at a rate of 50 sccm. Immediately after the 2-h long growth, the furnace was turned off, and the system was evacuated down to the base pressure of ~1.5 Torr. Additionally, the Ar flow was shut off and a 2 sccm flow of O₂ gas remained while the furnace cooled down to room temperature. Additional nanowires were grown in the conditions described in Ref. [37] (PbSn)Te nanowires were grown using the same CVD furnace through a vapor-liquid-solid mechanism with gold nanoparticles as the catalyst. PbTe powder (Alfa Aesar, purity 99.999%) and SnTe powder (Alfa Aesar, purity 99.999%) precursors were placed in alumina boats located in the middle of the upstream zones (i.e., zone 1 and 2), and Si substrates coated with 50 nm gold nanoparticles were placed in zone 3. Ar gas was flowed with a rate of 10 sccm, the growth pressure was 30 Torr, and the temperatures were set to 650, 710 and 575 °C for zone 1, 2 and 3, respectively.

2.2. Characterization

The SAED patterns were acquired using JEOL 1400Plus TEM at 120 kV, JEOL NEOARM TEM at 200 kV and JEOL 3200FS TEM at 300 kV. Focused ion beam was used to cut the nanowires into thin slices for TEM studies with the electron beam parallel to the nanowire axis. The 4D STEM was performed using the Thermo Fisher Titan at 300 kV with a 0.66 mrad cut-off angle and 145 mm camera length along with the electron microscope pixel array detector. Additional SAED patterns, Z-contrast STEM image, optimum bright-field images were taken using JEOL NEOARM TEM at 200 kV. The X-ray energy dispersive spectroscopy (EDX) were conducted by JEOL EDS system with dual SDD system. The quantification maps were generated using JED (JEOL EDS) software.

2.3. Theoretical calculation of scattering amplitude

We begin with an explicit form for the scattering amplitude,

$$S(\mathbf{q}) = \sum_{j=1}^{6} \sum_{i \mathbf{R}_i : 1} f_j \exp(i \mathbf{q} \cdot (\mathbf{R}_i + \mathbf{\tau}_j))$$
(1)

where f_j is the atomic structure factors of the Ir and O atoms and τ_j are their positions within the unit cell. $\{R_i\}$ represent positions of the unit cells making up the system. The sum is performed using a combination of analytic and numerical methods. In brief, because of the wire geometry, with sides at 45° angles relative to the high-symmetry directions, we started with a square cross-section and then eliminated unwanted sites. To do this we define

$$G_N(qa) \equiv \sum_{n=-N/2}^{N/2} exp(iqan)$$
 (2)

$$=\frac{\sin[qa(N+1)/2]}{\sin(qa/2)},\tag{3}$$

in terms of which one finds the scattering amplitude for the rectangular cross-section wire to be

$$S_0(\mathbf{q}) = \left[\sum_{j=1}^6 f_j \exp(i\mathbf{q}\cdot\tau_j)\right] \times G_{N_x}(q_x a) G_{N_y}(q_y a) G_{N_z}(q_z c). \tag{4}$$

We then remove parts of the rectangular lattice such that the resulting system has a cross-section with faces at 45° to the [100] and [010] axes of the underlying crystal. To do this we subtract

$$S_{P}(\mathbf{q}) = \left[\sum_{j=1}^{6} f_{j} \exp(i\mathbf{q} \cdot \tau_{j})\right] G_{N_{z}}(q_{z}c) \times \sum_{\{x_{i},y_{i}\} \in P} \exp[i(q_{x}x_{i} + q_{y}y_{i})],$$
 (5)

from the amplitude, where the last sum (over points in the removed regions, denoted by P) is numerically computed over all the unit cells being removed. For different choices of P, one can generate wires with a variety of cross-sectional geometries. The resulting scattering amplitude is given by $S(\mathbf{q}) = S_0(\mathbf{q}) - S_P(\mathbf{q})$. Note that a typical wire geometry studied in this work has $N_x = N_y = 240$, $N_z = 4800$.

3. Results and discussions

IrO₂ has a tetragonal rutile crystal structure as shown in Fig. 1(a). The as-grown nanowires are slightly tapered near the nanowire tip, which is seen clearly in a representative low-magnification TEM image taken with the electron beam perpendicular to the nanowire axis [Fig. 1] (b)]. By cutting the nanowires into thin slices using FIB, we performed further TEM studies with the electron beam parallel to the nanowire axis. As shown in Fig. 1(c) and S1(a), the nanowires have a truncatedrectangular cross-section, and the selected-area electron diffraction (SAED) [Fig. 1(d) and S1(c)] suggests that the wires are single crystals with a growth direction along the c-axis (or [001]) of the tetragonal crystal structure. The facets of the nanowire are found to be composed of four major {110} surfaces and four minor {100} surfaces, resulting in a slightly truncated-rectangular cross-section. The larger area of the {110} surfaces than the {100} facets are consistent with the surface energy calculations which indicate that the {110} family of planes are the most stable surfaces of the tetragonal IrO₂ phase [43]. The overall nanowire morphology and configurations of facets are illustrated in a schematic picture in the lower panel of Fig. 1(a). Atomic-resolution scanning TEM studies reveal the high crystalline quality of the IrO2 nanowires. Fig. 1(e) is an optimum bright-field (OBF) image showing the entire cross-section of the nanowire. At the corners, higher magnification OBF images were taken and displayed in Fig. 1(f)-(h). It is clearly seen in these figures that the {110} and {010} surfaces of the nanowire are atomically smooth and flat. Fig. 1(g) and (h) show the arrangement of the Ir and O atoms, which match with the projection of the tetragonal lattice of IrO₂ onto the plane.

Despite the high crystalline quality of the nanowires, a clear splitting of diffraction spots is observed in the SAED patterns that were taken with the e-beam along the b-axis (i.e. [010]). In this configuration [Fig. 1 (i)], the e-beam makes an angle of 45° with respect to the major facets (i. e. {110} surfaces), of the nanowires. The splitting of diffraction spots has the following characteristics: 1) the two spots in each pair have comparable intensity; 2) the split spots are separated in the [100] direction in reciprocal space, which is the diagonal direction of the nanowire cross-section; 3) the separation of the two split spots increases with the diffraction order (i.e., a larger separation for a higher miller index). Furthermore, the splitting of diffraction spots is strongly dependent on the relative orientation of the e-beam with respect to the facets. As shown in Fig. 1(j), the splitting evolves into long tails composed of multiple spots with varied intensities, when the beam is in the [120] zone axis which makes an angle of 26.6° (or 63.4°) to the major facets. No splitting is observed in the [110] zone axis, where the beam is perpendicular (or parallel) to the major facets. As shown in Fig. S2, a similar splitting phenomenon is also observed in the (PbSn)Te nanowires which have a rock-salt cubic crystal structure and a nearly rectangular cross section. In the case of (PbSn)Te, the major facets are the {100} surfaces which have the lowest surface energy, in contrast to the {110} for IrO₂. The splitting occurs most clearly when the e-beam makes an angle of 45° with the major facets, which in this case is the [110] zone axis of the rock-salt structure (in contrast to the [010] axis in the case of IrO₂). The two split spots are separated in the [100] direction in reciprocal space, which again corresponds to the diagonal direction of the nanowire cross-section. Therefore, the characteristics of the splitting are

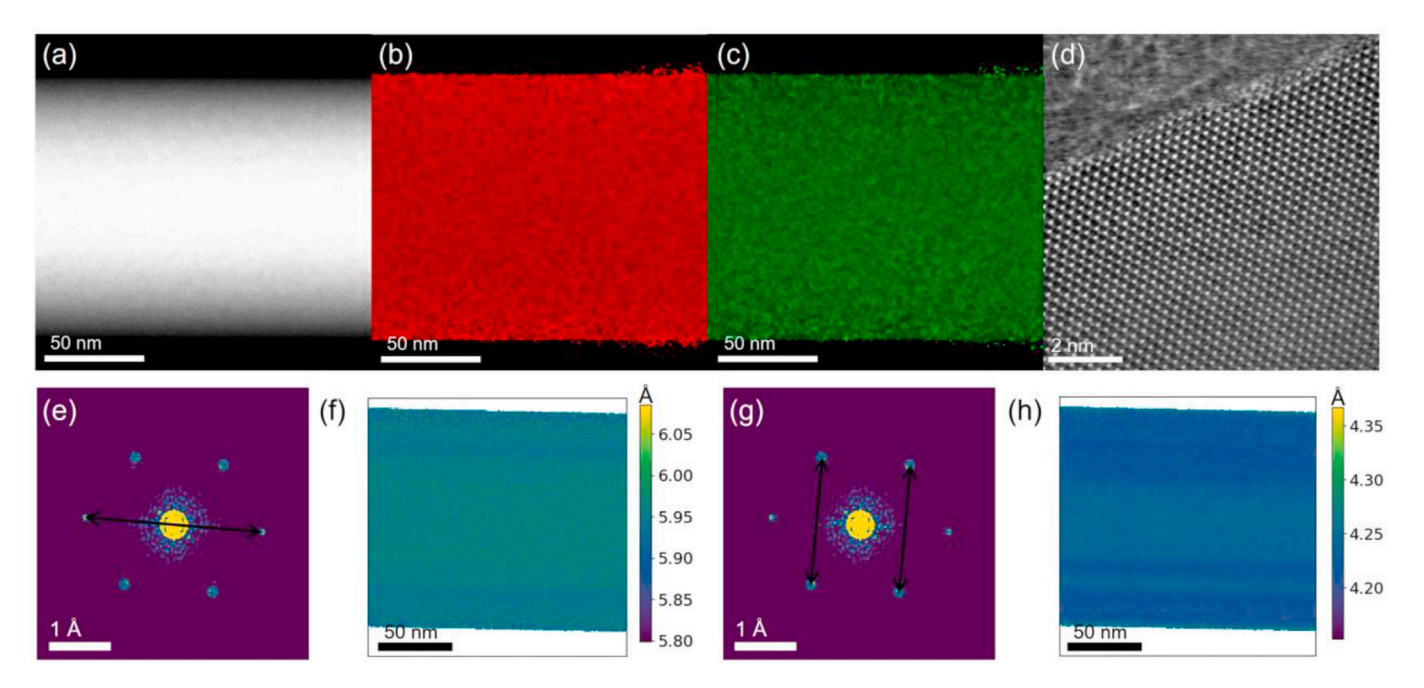


Fig. 2. (a) Z-contrast STEM image, EDX quantification maps of (b) O and (c) Ir elements of a IrO₂ nanowire segment. (d) OBF image of a IrO₂ nanowire with e-beam along [010] zone axis. (e)–(h) Strain mapping of a nanowire segment.

dependent on the relative orientation between the e-beam and the facets rather than the crystallographic orientation. This indicates the splitting is likely a geometric effect rather than an intrinsic material property (e. g., structural defects or inhomogeneity).

Compositional and structural inhomogeneities are further ruled out by elemental mapping using energy dispersive X-ray spectroscopy (EDS) and strain mapping using 4D scanning transmission electron microscopy (STEM) [44,45]. Fig. 2(a) shows a Z-contrast image of a nanowire segment with the e-beam in the [010] zone axis where the clearest splitting occurs in the SAED pattern. The variation in brightness confirms that the thickness varies across the diameter. EDS quantification maps taken in the same nanowire segment show fairly uniform distributions of both the Ir and O elements [Fig. 2(b) and (c)]. Atomic resolution OBF images were also taken in the [010] zone axis [Fig. 2(d)], which further confirm the high crystalline quality and surface smoothness of the IrO₂ nanowires. Strain maps were generated from 4D-STEM data, where a diffraction pattern was collected at every scanning point of

a STEM experiment. We reduced the aperture cut-off angle so that the scanning probe is a few nanometers in size, allowing us to sample several unit cells of the lattice and measure the local strain. To reduce the effect of uneven illumination of diffraction spots, we use cepstral analysis [46] which involves taking a power spectrum of every diffraction pattern. The resulting spots in the power spectrum can be interpreted as a pair-correlation function of the real-space lattice and the distance between spots represents the strain. As shown in Fig. 2(f) and (h), the strain maps are rather featureless, indicating the absence of notable strains.

Another possible origin of the splitting is the refraction of the e-beam at the surfaces of a regularly shaped crystal due to the different indices of refraction between the vacuum and the material [47,48]. This, however, is ruled out based on the following analysis: 1) The effect of electron refraction is notable only when the angle of incidence is nearly 90° (i.e., the e-beam is nearly parallel to the surface) due to the very small difference between the two indices of refraction of electrons in vacuum and in the material [47,48]. As described above, the splitting of diffraction

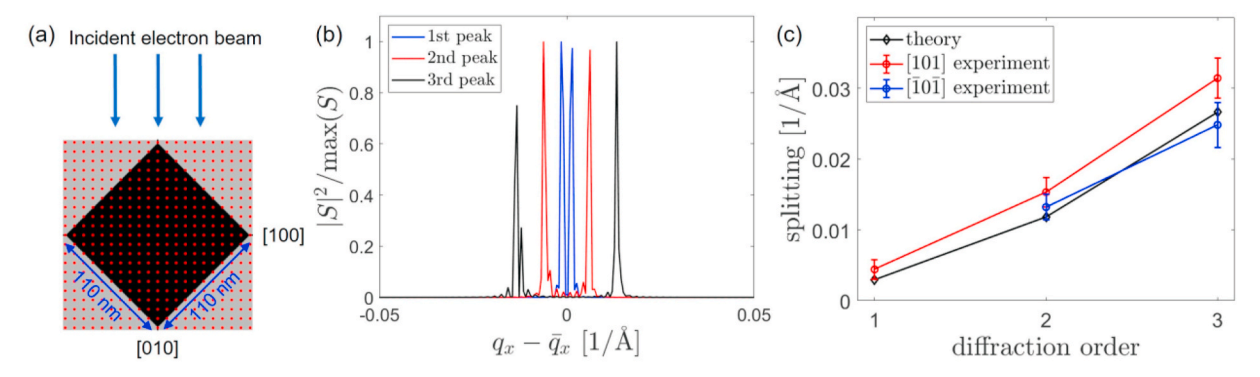


Fig. 3. (a) A schematic illustrating the cross-section of the nanowire. Crystal axes are at 45° angles relative to the direction normal to the wires surface. The electron beam is oriented in the [010] direction. A schematic of the underlying Bravais lattice is shown in red. For clarity the lattice density shown in the drawing is much sparser than the density of the actual nanowire used in the theoretical calculations and experiment. (b) The calculated intensity plots detailing how the 1st (blue), 2nd (red), and 3rd (black) peaks along the [101] direction split as a function of $q_x - \overline{q}_x$ where \overline{q}_x is the Bragg peak value of q_x . Plots are normalized such that they all have a maximum intensity of 1. (c) Peak splitting observed in an IrO₂ nanowire as a function of diffraction order for an energy of 300 keV. The diffraction order 1, 2, and 3 correspond to the miller indices: [101] ([$\overline{101}$]), [202] ([$\overline{202}$]), and [303] ([$\overline{303}$]), respectively. The two experimental results are slightly different from the numerical results (and from each other) due to a small but inevitable beam misalignment. The first diffraction order in the [$\overline{101}$] direction is not included because the splitting is too small for the camera to resolve.

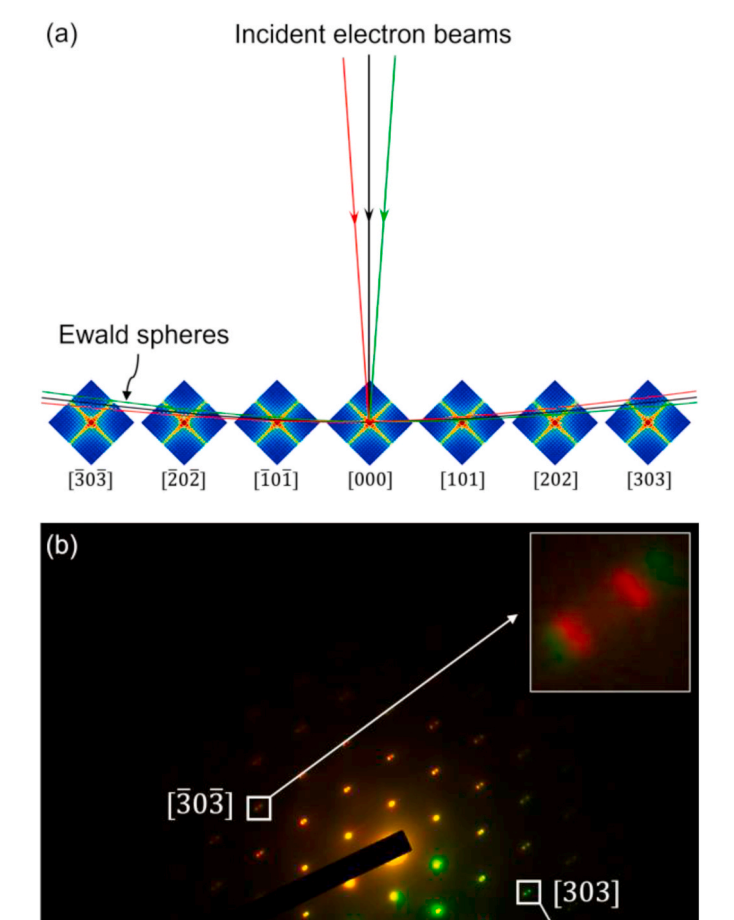


Fig. 4. (a) A schematic picture illustrating the intersection of Ewald spheres with the relrods in the reciprocal space. The black, green, and red curves denote the Ewald sphere with the e-beam along exactly the [010] zone axis, tilted slightly to the left, and to the right of the [010] axis, respectively. (b) Experimental results: two overlayed [010] SAED patterns of one IrO_2 nanowire acquired with the e-beam tilted to the left (red) and to the right (green).

10 1/nm

spots observed in the nanowires is the clearest when the incident angle is at 45° to the primary facets. At this relatively small incident angle, the deviation of electron beam as it passes through the nanowire is negligible. 2) While the incident angle of the beam at the two small {100} facets is $\sim\!90^\circ$, the separation between the two split spots caused by refraction is supposed to be nearly independent of the diffraction order, in strong contrast to the observation in shown Fig. 1(i), where the splitting increases with increasing diffraction order.

After eliminating the other possible mechanisms outlined above, we conclude that the best explanation for the observed splitting in the diffraction pattern is the geometric shape of the nanowire. A nanowire can be considered infinitely long in the axial direction when studying its SAED pattern, so that the configuration of relrods in reciprocal space is only determined by the cross section of the nanowire. For a nanowire with a nearly rectangular cross section, the geometric effect leads to a cross-like relrod configuration, where the rods in each cross are

perpendicular to the major facets. When the electron beam is along the [010] zone axis of an IrO_2 nanowire, it makes an angle of 45° with respect to the major facets; thus, the Ewald sphere intersects twice with each cross, resulting in the splitting of diffraction spots with splitting distances that increase with the diffraction order, due to the curvature of the Ewald sphere. On the other hand, when the e-beam is along [110] (*i. e.* parallel or perpendicular to the major facets), the Ewald sphere only intersects once with each cross, therefore no splitting is observed.

We followed the theoretical strategy outlined in Section 2.3 to compute the scattering amplitude. Fig. 3(a) illustrates the region used to compute $S(\mathbf{q})$ which in this case has a square cross section. The gray regions in this figure illustrate the points going into the computation of $S_P(\mathbf{q})$. The expressions for these quantities (Eq. (4) and (5)) can be numerically evaluated over a range of q to determine the diffraction pattern. We did this for a grid of q_x and q_z points, with q_y chosen by assuming the scattering process is elastic. A collection of intensity plots illustrating the splitting of the Bragg peaks is shown in Fig. 3(b). These plots were generated using a square wire of side length 110 nm and assuming an electron beam energy of 300 keV. For the same parameters, Fig. 3(c) shows the splitting distance as a function of diffraction order, showing good agreement with the experimental results obtained from an IrO2 nanowire using 300 keV TEM.

The geometric effect model is supported by the systematic changes of the splitting in the SAED patterns acquired with the e-beam slightly off the zone axis. As shown in a schematic picture in Fig. 4(a), the Ewald sphere intersects the relrods differently in the reciprocal space when the e-beam is tilted away from the zone axis. To be more specific, when the e-beam is tilted slightly to the left (red), the separation between the split spots on the left side (e.g., $[\overline{3}0\overline{3}]$) will decrease while the ones on the right side (e.g., [303]) will increase. The opposite would occur if the beam were tilted to the right (green). This is exactly what is experimentally observed in Fig. 4(b), where two sets of SAED patterns (green and red) taken from an IrO2 nanowire with different tilting orientations are overlayed. For example, the separation between the two $[\overline{3}0\overline{3}]$ spots is larger when the e-beam is tilted to the right (green), whereas the separation between the two [303] spots is larger when the e-beam is tilted to the left (red). The model is further supported by the observation of streaks in Fig. 1(d). When the e-beam is along the nanowire axis, i.e. perpendicular to the cross section of the nanowire, the wave vector of the incident e-beam is also perpendicular to the plane of the cross in reciprocal space. Therefore, the intersection of the Ewald sphere with the reciprocal cross inherits a cross-like shape, showing perpendicular streaks in the diffraction spots. It is worth noting that the streaks observed in Fig. 1(d) are in directions perpendicular to the sides of the cross section in Fig. 1(c), which is consistent with the fact that the relrods, due to the geometric effect, are perpendicular to the corresponding sides of the rectangular cross-section.

We further show the feasibility of utilizing the observed effect to decode information about the wire geometry. As shown in Fig. 5(a), the Ewald sphere intersects with only one relrod when the e-beam is perpendicular to the two parallel facets of a nanowire with a rectangular cross-section. The intensity on the relrod oscillates at a period of $\Delta q =$ 1/t, where *t* is the thickness of the nanowire along the e-beam direction. When the e-beam is gradually tilted away from the zone axis, a series of Ewald spheres intersect with the relrod at different locations, resulting in an oscillation of diffraction intensity. Such an oscillation was observed in the SAED patterns, which were taken with the e-beam tilted away from the [110] zone axis of an IrO₂ nanowire [Fig. 5(b)-(h)]. The rotation axis for tilting is approximately along the nanowire axial direction, and θ is the tilt angle measured from the [110] zone axis. To minimize the influence of offset between the rotational axis and the nanowire axis, we consider the $(1\overline{1}0)$ and $(\overline{1}10)$ spots which are perpendicular to the nanowire axial direction. The oscillation period Δq was calculated to be $\sim 0.014~\text{nm}^{-1}$ based on an estimation of $\Delta heta \sim 0.25^\circ$, as discussed in the SI. This corresponds to a thickness t=70

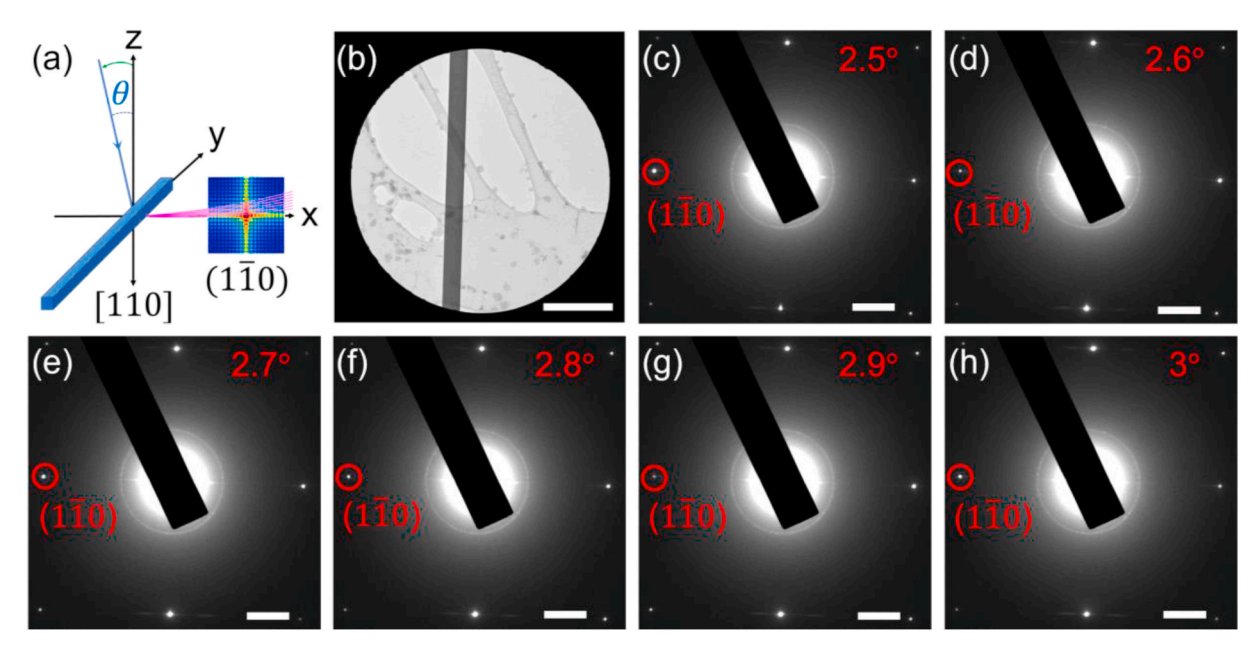


Fig. 5. (a) A schematic picture illustrating the intersection of Ewald spheres with a relrod when the e-beam is slightly tilted away from the zone axis [110] by an angle θ which is illustrated by the blue arrow. The magenta arcs represent part of the Ewald spheres with different tilting angles. The x, y and z axes are along [1 $\overline{10}$], [001] and [110] directions respectively. (b) A low-magnification TEM image showing the selected area where the diffraction patterns were taken. The scale bar is 500 nm. (c)–(h) are the diffraction patterns at a series of successive θ with a step size of 0.1°, where the intensity of (1 $\overline{10}$) spot oscillates. The scale bar is 1 1/nm.

nm, which is consistent with the measurement by SEM [Fig. S4].

Finally, we note that an analogous geometric effect was previously reported in quasi-0-dimensional nanoparticles [49–51]. Since the nanoparticles are confined in all three dimensions (3D), the configuration of their relrods would be 3D as well. The intersection of the 3D rods with the Ewald sphere gives rise to 2D patterns or streaks around the diffraction spots. On the other hand, 1D nanowires can be considered infinitely long in the axial direction, such that all the relrods lie in the cross-sectional plane perpendicular to the nanowire axis. Thus, in the SAED patterns of nanowires, the geometric effect only induces fine structure for each diffraction spot along directions perpendicular to the axis of nanowire, which may be a reason why this effect was largely overlooked.

4. Conclusions

In summary, we report on the first experimental observation of a geometric effect on electron diffraction in 1D nanostructures, via systematic transmission electron microscopy studies in combination with theoretical simulations. The effect is manifested by a zone axis dependent splitting of diffraction spots observed in single-crystalline nanowires of two representative materials IrO2 and (PbSn)Te with nearly rectangular cross-section. Detailed structural and compositional characterizations and analysis at the atomic scale rule out other possible origins for the splitting, leaving the geometric effect the only feasible mechanism. This is further supported by theoretical simulations of the observed splitting. We note that the geometric effect in 1D nanowires is less obvious than in quasi-0-D nanoparticles and can be easily overlooked or mistakenly attributed to other origins. The unambiguous observation of geometric effect in this work offers a non-destructive approach to characterizing the cross-sectional size and geometry of one-dimensional nanostructures, which strongly influence their physical and chemical properties.

Credit author statement

Tongxie Zhang: Formal analysis, Investigation, Writing – original draft **Adam Eaton:** Formal analysis, Methodology, Writing – original

draft **Dibya Mukherjee**: Formal analysis, Methodology, Writing – review & editing **Michael Cao**: Formal analysis, Investigation, Writing – original draft **Amanda Coughlin**: Investigation, Writing – review & editing **Thomas Ruch**: Investigation, Writing – review & editing **Xun Zhan**: Investigation, Writing – review & editing **Hanyu Zhu**: Formal analysis, Writing – review & editing **Yimo Han**: Supervision, Writing – review & editing **Herbert Fertig**: Methodology, Supervision, Writing – original draft **Shixiong Zhang**: Conceptualization, Supervision, Writing – original draft

Declaration of competing interest

The authors declare that they have no known competing financial interests or personal relationships that could have appeared to influence the work reported in this paper.

Data availability

Data will be made available on request.

Acknowledgements

We thank Prof. J. Wang, Dr. D.Y. Xie, Dr. H. Sawada, and Prof. D. Muller for helpful discussions. The authors are also grateful to JEOL for taking some of the SAED patterns, Z-contrast STEM image, OBF images for us. We acknowledge the financial support from Indiana University College of Arts and Sciences (start-up support) and the U.S. National Science Foundation (ECCS-1936406, DMR-1914451 and DMR-2005096). M.C. and Y.H. acknowledge the support from Welch Foundation (C-2065-20210327). We also thank the Indiana University-Bloomington Electron Microscopy Center for access to transmission electron microscope and Nanoscale Characterization Facility for access to scanning electron microscope.

Appendix A. Supplementary data

Supplementary data to this article can be found online at https://doi.org/10.1016/j.mtphys.2023.101048.

References

- [1] W. Lu, C.M. Lieber, Nat. Mater. 6 (2007) 841.
- [2] O. Hayden, R. Agarwal, W. Lu, Nano Today 3 (2008) 12.
- [3] N.P. Dasgupta, J. Sun, C. Liu, S. Brittman, S.C. Andrews, J. Lim, H. Gao, R. Yan, P. Yang, Adv. Mater. 26 (2014) 2137.
- [4] C. Jia, Z. Lin, Y. Huang, X. Duan, Chem. Rev. 119 (2019) 9074.
- [5] T. Sannicolo, M. Lagrange, A. Cabos, C. Celle, J.P. Simonato, D. Bellet, Small 12 (2016) 6052.
- [6] L.N. Quan, J. Kang, C.-Z. Ning, P. Yang, Chem. Rev. 119 (2019) 9153.
- [7] P. Christopher, S. Linic, J. Am. Chem. Soc. 130 (2008): 11264.
- [8] C. Koenigsmann, A.C. Santulli, K. Gong, M.B. Vukmirovic, W.-p. Zhou, E. Sutter, S. S. Wong, R.R. Adzic, J. Am. Chem. Soc. 133 (2011) 9783.
- [9] I. Paramasivam, H. Jha, N. Liu, P. Schmuki, Small 8 (2012) 3073.
- [10] H. Xu, H. Shang, C. Wang, Y. Du, Adv. Funct. Mater. 30 (2020): 2000793.
- [11] A.I. Hochbaum, P. Yang, Chem. Rev. 110 (2010) 527.
- [12] J.S. Chen, X.W. Lou, Small 9 (2013) 1877.
- [12] S.S. Gard, A.W. Edward, Shinai V. Gutta, S. Gard, A.W. Edward, A.
- [15] G. Otnes, M.T. Borgström, Nano Today 12 (2017) 31.
- [16] S.-H. Lee, Y. Jung, R. Agarwal, Nat. Nanotechnol. 2 (2007) 626.
- [17] J.I. Sohn, S.S. Choi, S.M. Morris, J.S. Bendall, H.J. Coles, W.-K. Hong, G. Jo, T. Lee, M.E. Welland, Nano Lett. 10 (2010) 4316.
- [18] J.K. Hyun, S. Zhang, L.J. Lauhon, Annu. Rev. Mater. Res. 43 (2013) 451.
 [19] S. Nauert, A. Paul, Y.-R. Zhen, D. Solis Jr., L. Vigderman, W.-S. Chang, E. R. Zubarev, P. Nordlander, S. Link, ACS Nano 8 (2014) 572.
- [20] M. Li, Z. Zhao, T. Cheng, A. Fortunelli, C.-Y. Chen, R. Yu, Q. Zhang, L. Gu, B. V. Merinov, Z. Lin, Science 354 (2016) 1414.
- [21] R.D. Abdel-Rahim, M.Y. Emran, A.M. Nagiub, O.A. Farghaly, M.A. Taher, Electrochem. Sci. Adv. 1 (2021): e2000031.
- [22] S. Yin, G. Cheng, G. Richter, H. Gao, Y. Zhu, ACS Nano 13 (2019) 9082.
- [23] L.M. Vogl, P. Schweizer, G. Richter, E. Spiecker, MRS Adv. 6 (2021) 665.
- [24] G. Xiao-Kun, C. Bing-Yang, Chin. Phys. 16 (2007) 3777.
- [25] J. Chen, G. Zhang, B. Li, J. Chem. Phys. 135 (2011): 204705.
- [26] Q. Zhang, C. Liu, X. Liu, J. Liu, Z. Cui, Y. Zhang, L. Yang, Y. Zhao, T.T. Xu, Y. Chen, J. Wei, Z. Mao, D. Li, ACS Nano 12 (2018) 2634.
- [27] T.H. Hsieh, H. Lin, J. Liu, W. Duan, A. Bansil, L. Fu, Nat. Commun. 3 (2012) 1.
- [28] J. Liu, W. Duan, L. Fu, Phys. Rev. B 88 (2013): 241303.
- [29] B.J. Wieder, B. Bradlyn, J. Cano, Z. Wang, M.G. Vergniory, L. Elcoro, A. A. Soluyanov, C. Felser, T. Neupert, N. Regnault, B.A. Bernevig, Nat. Rev. Mater. 7 (2022) 196.

- [30] Y. Ding, Z. L. Wang, Vol. 108, ACS Publications, 2004.
- [31] C.S. Kumar, Transmission Electron Microscopy Characterization of Nanomaterials, Springer Science & Business Media, 2013.
- [32] H. Zheng, MRS Bull. 46 (2021) 443.
- [33] D.B. Williams, C.B. Carter, Transmission Electron Microscopy, Springer, 1996.
- [34] Y. Sun, Y. Zhang, C.-X. Liu, C. Felser, B. Yan, Phys. Rev. B 95 (2017): 235104.
- [35] J. Nelson, J. Ruf, Y. Lee, C. Zeledon, J. Kawasaki, S. Moser, C. Jozwiak, E. Rotenberg, A. Bostwick, D. Schlom, K.M. Shen, L. Moreschini, Phys. Rev. Mater. 3 (2019): 064205.
- [36] X. Xu, J. Jiang, W. Shi, V. Süß, C. Shekhar, S. Sun, Y. Chen, S.-K. Mo, C. Felser, B. Yan, H. Yang, Z. Liu, Y. Sun, L. Yang, Y. Chen, Phys. Rev. B 99 (2019): 195106.
- [37] Y. Tao, Z. Pan, T. Ruch, X. Zhan, Y. Chen, S. Zhang, D. Li, Mater. Today Phys. 21 (2021): 100517.
- [38] A.L. Coughlin, Z. Pan, J. Hong, T. Zhang, X. Zhan, W. Wu, D. Xie, T. Tong, T. Ruch, J.J. Heremans, J. Bao, H.A. Fertig, J. Wang, J. Kim, H. Zhu, D. Li, S. Zhang, Adv. Sci. (2022): 2204424.
- [39] S.-Y. Xu, C. Liu, N. Alidoust, M. Neupane, D. Qian, I. Belopolski, J. Denlinger, Y. Wang, H. Lin, L. Wray, G. Landolt, B. Slomski, J. Dil, A. Marcinkova, E. Morosan, Q. Gibson, R. Sankar, F. Chou, R. Cava, A. Bansil, M. Hasan, Nat. Commun. 3
- [40] J. Liu, T.H. Hsieh, P. Wei, W. Duan, J. Moodera, L. Fu, Nat. Mater. 13 (2014) 178.
- [41] E. Xu, Z. Li, J.A. Acosta, N. Li, B. Swartzentruber, S. Zheng, N. Sinitsyn, H. Htoon, J. Wang, S. Zhang, Nano Res. 9 (2016) 820.
- [42] A. Zhang, F. Wei, C. Yan, F. Wang, S. Ma, Z. Zhang, Nanotechnology 30 (2019):
- [43] G. Novell-Leruth, G. Carchini, N. López, J. Chem. Phys. 138 (2013): 194706.
- [44] C. Ophus, P. Ercius, M. Sarahan, C. Czarnik, J. Ciston, Microsc. Microanal. 20 (2014) 62.
- [45] M.W. Tate, P. Purohit, D. Chamberlain, K.X. Nguyen, R. Hovden, C.S. Chang, P. Deb, E. Turgut, J.T. Heron, D.G. Schlom, D.C. Ralph, G.D. Fuchs, K.S. Shanks, H. T. Philipp, D.A. Muller, S.M. Gruner, Microsc. Microanal. 22 (2016) 237.
- [46] E. Padgett, M.E. Holtz, P. Cueva, Y.-T. Shao, E. Langenberg, D.G. Schlom, D. A. Muller, Ultramicroscopy 214 (2020): 112994.
- [47] J. Cowley, A. Rees, Nature 158 (1946) 550.
- [48] H. Raether, Nature 161 (1948) 311.
- [49] Y. Ding, Y. Gao, Z.L. Wang, N. Tian, Z.-Y. Zhou, S.-G. Sun, Appl. Phys. Lett. 91 (2007): 121901.
- [50] R. Dronyak, K.S. Liang, J.-S. Tsai, Y.P. Stetsko, T.-K. Lee, F.-R. Chen, Appl. Phys. Lett. 96 (2010): 221907.
- A.B. Shah, S.T. Sivapalan, B.M. DeVetter, T.K. Yang, J. Wen, R. Bhargava, C. J. Murphy, J.-M. Zuo, Nano Lett. 13 (2013) 1840.